

PCCP

Accepted Manuscript



This is an *Accepted Manuscript*, which has been through the Royal Society of Chemistry peer review process and has been accepted for publication.

Accepted Manuscripts are published online shortly after acceptance, before technical editing, formatting and proof reading. Using this free service, authors can make their results available to the community, in citable form, before we publish the edited article. We will replace this *Accepted Manuscript* with the edited and formatted *Advance Article* as soon as it is available.

You can find more information about *Accepted Manuscripts* in the [Information for Authors](#).

Please note that technical editing may introduce minor changes to the text and/or graphics, which may alter content. The journal's standard [Terms & Conditions](#) and the [Ethical guidelines](#) still apply. In no event shall the Royal Society of Chemistry be held responsible for any errors or omissions in this *Accepted Manuscript* or any consequences arising from the use of any information it contains.

Temperature Dependent Structural Variations of $\text{OH}^-(\text{H}_2\text{O})_n$ $n=4-7$: Effects on Vibrational and Photoelectron Spectra

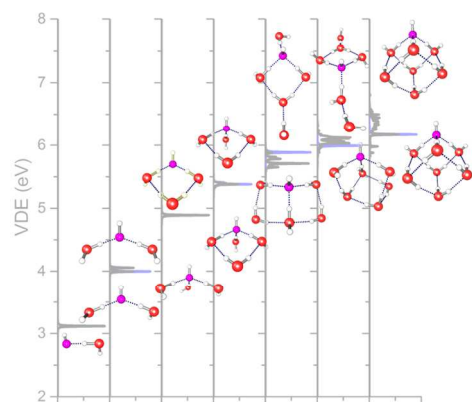
Ren-Jie Lin,^{1‡} Quoc Chinh Nguyen,^{2‡} Yew-Soon Ong,³ Kaito Takahashi^{1*} and Jer-Lai Kuo^{1*}

¹Institute of Atomic and Molecular Sciences, Academia Sinica, Taipei 10617, Taiwan)

²School of Physical and Mathematical Sciences, Nanyang Technological University, 637371, Singapore

³School of Computer Engineering, Nanyang Technological University, 639798, Singapore

TOC GRAPHICS



ABSTRACT

In this work, we identified a large numbers of structurally distinct isomers of midsized deprotonated water clusters, $\text{OH}^-(\text{H}_2\text{O})_{n=4-7}$, using first-principles methods. Temperature dependence of the structural variation in the solvation shell of OH^- for these clusters were examined with harmonic superposition approximation. We simulated the vibrational and photoelectron spectra based on these thermodynamic calculations. We found that the isomers with 3-coordinated hydroxide dominate the population in these midsized clusters. Furthermore, increase in temperature causes the topological change from compact isomers with many intermolecular hydrogen bonding to open isomers with fewer but directional intermolecular hydrogen bonds. We showed that this evolution in structure can be observed through the change in the vibrational spectra at 3200-3400 cm^{-1} . In addition, the increase in directional hydrogen bonded isomers, which have outer hydration shell with OH bonds pointing to the hydroxide, causes the vertical detachment energy to increase at higher temperatures. Lastly, we also performed studies to understand the variation in the aforementioned spectral quantities with the variation in the coordination number of the hydroxide.

I. INTRODUCTION

Protons and hydroxide play an important role in acid base chemistry. However, the detailed solvation structure of the hydroxide is still not clearly understood.^{1,2,3,4,5,6,7,8,9} Experimental studies on deprotonated and protonated water clusters have been performed to remedy this problem.^{10,11,12,13,14,15} Yang et al.¹⁶ produced large-sized clusters of $\text{OH}^-(\text{H}_2\text{O})_{n=0-59}$ and discovered “magic numbers” at $n = 11, 14, 17$ and 20 . In the last decade, numerous theoretical studies^{17,18,19,20,21,22,23} have been made to reveal the optimal structures, the vibrational frequencies, and the role of the first solvation shell of OH^- anions toward proton transfer. Several experimental researches have attempted to obtain the structures and hydrogen bonding patterns of $\text{OH}^-(\text{H}_2\text{O})_n$ via infrared spectroscopic measurements.^{14,24,25} Chaudhuri and coworkers,²⁵ systematically examined the infrared spectra of $\text{OH}^-(\text{H}_2\text{O})_{n=1-5}$ both experimentally and theoretically with DFT calculations. Robertson et al. identified signatures of open hydration shell for hydroxide anion and also observed spectral features that signify the formation of the second solvation shell.¹⁴

The increased intensive activities on accurate experimental studies of small-sized clusters have led to significant theoretical effort in this field.^{17,18,19,20,21,22,23,26} Nevertheless, there are limited simulation studies that bring insights into the morphological transitions of deprotonated water clusters. In the present work, we endeavor to fill this gap by investigating the equilibrium structures, relative stability, vibrational and photoelectron spectra of $\text{OH}^-(\text{H}_2\text{O})_n$ from small to mid sizes of $n = 4-7$. In our study, numerous isomers have been identified at different levels of first-principle calculations. Thermodynamic characteristics were subsequently derived in conjunction with vibrational analysis. In the present study we placed emphasis on the evolution of structural features and hydrogen bonding network as a function of temperature. Utilizing the

computed vibrational peak positions and intensities we simulate the vibrational spectra. Furthermore, we provide characteristic peak positions for the fairly stable cubic isomer of OH^- (H_2O)₇, which has yet been observed experimentally.

On the other hand, hydration of the hydroxide can greatly alter its electronic state as can be observed in the photoelectron spectra. The gas phase electron detachment energy of OH^- has been measured to be 1.8 eV²⁷, however it massively increases to 9.2 eV in aqueous phase, according to photoelectron spectroscopy using liquid jet apparatus.²⁸ Previously, one of the authors have performed density functional calculation on the first vertical detachment energy (VDE) for select isomers of smaller sized clusters $n=0-5$ and saw a gradual increase in VDE from 1.8 to 6.0 eV.²⁹ In the present study, a more thorough study is performed including 1. larger clusters, 2. thermal effects, as well as 3. studies on the second and third VDE. By detailed examination of the temporal evolution of the photoelectron spectra, we intend to glean into the solvation effect caused by the water molecules. Especially we will evaluate how the observable varies with the number of the first solvation shell, the coordination number of the hydroxide. Furthermore, we clarify how the change in the second and outer solvation shell will affect the photoelectron spectra.

The rest of the paper is organized in the following manner. In section II, the details for the theoretical methods will be given. In section III, we present the results and analysis of the theoretical calculations. Lastly we provide a brief conclusion in section IV.

II. METHODOLOGY

A. Hierarchical exploration of energy landscape of $\text{OH}^-(\text{H}_2\text{O})_{4-7}$

We employed an hierarchical approach for an efficient and extensive exploration on the potential energy surface (PES) of $\text{OH}^-(\text{H}_2\text{O})_{n=4-7}$. This hierarchical search approach has been previously used in the analysis of pure³⁰ and protonated³¹ water clusters by some of us. In this work, we first identified various structural isomers with OSS2 model, an empirical potential³², in conjunction with an asynchronous memetic algorithm.^{33,34} Local minima of the isomers were then refined using density functional theory with Becke's 3 parameter hybrid functional (B3LYP)^{35,36} with the 6-31+G(d) basis.^{37,38,39,40} After the preliminary optimizations, all of the duplicated minima were filtered out by ultrafast shape recognition metric, developed by Ballester and Richards.⁴¹ Since anion clusters normally require a larger basis set for a better description on the delocalized electron, we have then re-optimized all isomers with B3LYP/6-311+G(d,p) for the following discussions.

The purpose of synergizing the empirical model with first-principle calculations is to benefit the efficiency of empirical model in identifying the isomers whereas the most time consuming part, first-principle optimization, is then executed on parallel compute clusters. It is however important to note that the OSS2 empirical potential failed to obtain 5-coordinated isomers which were previously mentioned in the literature.²² Therefore, we manually added 5-coordinated species to the calculation when performing the optimization with B3LYP/6-311+G(d,p). All the B3LYP calculations including optimization and harmonic vibrational analysis were performed using the Gaussian09 suite package.⁴² The vibrational frequencies for the IR and Raman spectra

were scaled by a factor of 0.9730.⁴³ The IR spectra for each isomer was calculated using the equation

$$I^{IR}(\omega) = \sum_i^{n_{vib}} I_i L(\omega_i, \Gamma_i), \quad (1)$$

where ω_i and I_i are the peak angular frequency and fundamental integrated absorption coefficient for vibrational mode i obtained from the Gaussian09 program. L is a normalized Lorentzian function with width Γ_i that is centered at ω_i . The Raman cross section, ignoring the excitation laser frequency, for each isomer was calculated using the following equation⁴⁴:

$$I^{Raman}(\omega) = \sum_i^{n_{vib}} \frac{1}{1 - e^{-\hbar\omega_i/k_B T}} \frac{A_i}{\hbar\omega_i} L(\omega_i, \Gamma_i), \quad (2)$$

where A_i is the Raman activity calculated by the Gaussian09 program. Since most of the experiments are performed in the frequency range of the OH stretching modes, we report the vibrational spectra in the 2000-3700 cm^{-1} range.

B. Harmonic superposition approximation

From the collection of optimized isomers, the structural transitions and thermodynamic properties of water clusters can then be analyzed by using harmonic superposition approximation (HSA). HSA represents an effective approach for acquiring the diverse physical properties of a system from the collection of isomers as opposed to exploring on the potential energy landscape directly. The underlying theory is to treat each local minimum as a harmonic and infinite basin characterized by vibrational frequencies and relative energies. The total partition function and observable quantities of the system are subsequently derived as a summation of the contributions from the isomers.^{45,46,47,48,49,50,51} It is worth highlighting that the accuracy of the approach greatly

depends on the fidelity and completeness of the obtained isomers. Therefore, an effective multi-modal global search algorithm is crucial for identifying the complete or near complete isomer sets. Additionally, the harmonic vibration analysis is used to retrieve the vibrational frequencies of each identified isomers. HSA represents a reasonable choice for examining the equilibrium properties since its approximation accuracy is significantly close to conventional MC-based algorithms' as demonstrated in the previous studies on protonated water cluster and other related studies.^{30,50}

C. Vertical Detachment Energy

To calculate the vertical detachment energy (VDE) of $\text{OH}^-(\text{H}_2\text{O})_n$, we perform calculation for neutral $\text{OH}(\text{H}_2\text{O})_n$ radical at the respective hydrated hydroxide cluster geometry. Using the anion geometries optimized by B3LYP/6-311+G(d,p) the 1st VDE can be obtained by calculation of the neutral species using UB3LYP/6-311+G(d,p) and taking the energy difference. For bare OH^- , the detachment of the excess electron can occur from the Π symmetry highest occupied molecular orbital which are the degenerate $2p_x$ and $2p_y$ orbitals of the oxygen atom (where z-axis is along the OH bond). Thereby the 1st and 2nd VDE will be seen at the same energies. On the other hand the 3rd detachment will be from the Σ molecular orbital mainly consisting of the $2p_z$ orbital which will have a much higher energy. In order to determine the variation in the detachment from different molecular orbitals we performed equation of motion couple cluster singles and doubles ionization (EOM-CCSD-IP)^{52,53} calculation using the $\text{OH}^-(\text{H}_2\text{O})_n$ geometries calculated using B3LYP/6-311+G(d,p). This EOM-CCSD-IP/6-311+G(d,p) calculation for 4 excited states was performed using the Q-Chem program.⁵⁴ To examine the variance in the VDE as a function of n , we have performed VDE calculation for $n = 0-7$, where the geometries for $n=0-4$ species were also optimized using the B3LYP/6-311+G(d,p). Since the detailed

geometries of these smaller species are reported previously they will not be discussed in the present paper, and we will concentrate on the size dependence of VDE in this paper. We note that for proper treatment of the photoelectron spectra, the ionization efficiency for different excitations should be considered, however since this is beyond the scope of this paper, we use unity ionization efficiency to plot the spectra.

III. RESULTS AND DISCUSSIONS

A. Low-energy isomers

The sets of 20, 66, 169 and 696 distinct isomers of $\text{OH}^-(\text{H}_2\text{O})_n$ for $n = 4 - 7$, respectively, are identified at B3LYP/6-311+G(d,p) using the hierarchical search approach described in Section II A. According to the compactness of topological geometries, all isomers are classified into five structural categories, namely, multi-ring (MR), double-ring (DR), single-ring (SR), tree-like (T), and linear (L) forms. Structure and relative energy of low-energy isomers of each category are depicted in Fig. 1. In the present study we only observe isomers where the water molecule is coordinated to the oxygen atom of the hydroxide. Generally speaking, due to the largest number of hydrogen bonding, the compact DR and MR topologies usually have the lowest electronic energy. The more open SR, T and L topologies have higher electronic energies, but they have many more low frequency vibrational modes.

Here we first validate the accuracy of the relative energetics obtained by B3LYP/6-311+G(d,p). For $\text{OH}^-(\text{H}_2\text{O})_4$, the electronic energy difference between the most stable DR-I (3-coordinated) and T-I (4-coordinated) is 0.54 kcal/mol, which is much smaller than the 1.48 kcal/mol obtained by the smaller basis B3LYP/6-31+G(d) (see Fig. S1 in supplementary material

for details). Previously we have used MP2/6-311++G(3df,3pd) and obtained an energy difference of 0.62 kcal/mol.⁵⁵ Furthermore, Sun et al. used CCSD(T) method and obtained 0.35 kcal/mol, thereby showing the importance of including bigger basis sets to correctly describe the floppy ionic hydrogen bond (IHB) between the hydroxide and water.²² As for the $\text{OH}^-(\text{H}_2\text{O})_5$, we find that the 5-coordinated isomer is 4.4 kcal/mol higher in electronic energy compared to the most stable MR (3-coordinated) isomer. Previously, Sun et al. reported that the 5-coordinated isomer is 3.03 kcal/mol higher in energy compared to the 4-coordinated isomer using MP2/aug-cc-pVQZ. Furthermore, they report that the 5-coordinated isomer is isoenergetic to the 3-coordinated isomer with that level of quantum chemistry. These results contradict with our present studies, but this is due the different isomer used in the calculations of Sun et al. They did not perform a thorough search in the geometry space to obtain all the possible isomers, so the 4-coordinated isomer reported in their paper is not the most stable isomer in our collection of isomers.

Since there are no other systematic study on the larger size clusters for comparison, we have performed single point calculations using MP2/6-311+G(d,p) and CCSD/6-311+G(d,p) at the B3LYP/6-311+G(d,p) optimized geometries and confirmed that the relative energies are consistent (see Fig. S2 in supplementary material). In conclusion we believe that the ordering of the electronic energies of the different topologies are accurate to give correct thermal behavior for the clusters studied in the present study.

B. Thermal behaviors

The thermal behaviors of deprotonated water clusters are investigated by calculating the canonical heat capacity using HSA.³⁰ The population or canonical probability of each topology is

subsequently calculated as a function of temperature when studying the structural transitions. Fig. 2 shows the HSA simulation results of $\text{OH}^-(\text{H}_2\text{O})_{n=4-7}$ based on the B3LYP/6-311+G(d,p) energetics and vibrational frequencies. From the trend of the pink dotted line, one can notice that the most stable isomer dominates population at low temperatures.

The HSA result of $\text{OH}^-(\text{H}_2\text{O})_4$ is depicted in Fig. 2a and we can observe a single structural transition between SR and T isomers at around 200 K. While the most stable isomer, shown in the left hand side of Fig 2a, dominate the population at temperature less than 50K, at higher temperatures a few SR isomers can co-exist. Above 200 K the T topology start to dominate, but most of these T isomers are 3-coordinated, and 4-coordinated T isomers only have a population of $\sim 1\%$ at maximum in the temperature range we studied here. This is because among the 20 isomers of $\text{OH}^-(\text{H}_2\text{O})_4$, there are two 4-coordinated, twelve 3-coordinated and six 2-coordinated structures. Due to the large number of possible structures, the population is dominated, $\sim 97\%$, by these 3-coordinated isomers. For $\text{OH}^-(\text{H}_2\text{O})_5$, we can see in Fig. 1 that while MR-I has the lowest electronic energy, DR-II of $\text{OH}^-(\text{H}_2\text{O})_5$ is energetically favorable after adding zero-point correction. The relative energetics between these two types of isomer is consistent with the thermal population shown in Fig. 2(b) in which we can see DR dominate the population until $\sim 75\text{K}$ before giving ways to SR and then at $\sim 250\text{K}$ T takes over. Similar to $n=4$, among the 66 isomers in $\text{OH}^-(\text{H}_2\text{O})_5$, the majority, fifty-nine, have 3-coordinated structures. Of the remaining seven isomers, three of them are 2/4-coordinate structures and there is only one 5-coordinated structure. Thus most of the population studied in the present temperature range are dominated by the 3-coordinated isomers. For $\text{OH}^-(\text{H}_2\text{O})_6$ and $\text{OH}^-(\text{H}_2\text{O})_7$, given in Fig. 2(c) and 2 (d), the characteristics of the population is similar where the MR isomers dominate the population at low temperature which is then followed by the emergence of DR and SR isomers. Similar to smaller

cases the 3-coordinated isomers dominate the population and we see minimal 4- and 5-coordinated structures in the population. It is worthwhile mentioning that in $\text{OH}^-(\text{H}_2\text{O})_7$, the most stable cubic isomer, shown in the left of Fig 2d, dominate the population (more than 75%) up to 150K. Therefore we believe that this isomer will be experimentally accessible and we report the vibrational and photoelectron spectra for this fairly stable “smallest basic ice cube” in the next sections.

C. Vibrational IR spectra and Raman scattering

The vibrational spectrum, $I_{total}(\omega)$, is calculated as the sum of the spectrum of each individual isomer weighted by its corresponding canonical probability as follows:

$$I_{total}(\omega) = \sum_a I_a(\omega) p_a(T), \quad (3)$$

where the sum is taken for all distinct isomers we identified, $I_a(\omega)$ is the spectrum of isomer a derived from the vibrational analysis given in eq (1) and (2), $p_a(T)$ denotes the canonical probability computed by HSA as discussed in Section III B. The homogeneous widths for free OH modes were set to 20 cm^{-1} . For the hydrogen bonded OH stretching, we adopt the power law formula derived previously. For $\text{OH}^-(\text{H}_2\text{O})_n$, $n=2-4$, we previously performed on-the-fly simulation to determine the OH stretching fundamental vibrational energy decay life time. We found that the theoretical vibrational decay lifetime can be fit to a power law relation to the red shift of hydrogen-bonded OH stretching peak.⁵⁵ Since the homogeneous width, Γ , can be written as the inverse of the decay life time, $\Gamma = \alpha (\omega_\phi - \omega)^\beta$, where $\Delta\omega = \omega_\phi - \omega$ is the red shift, in wavenumbers, of the hydrogen bonded OH band peak with respect to the free OH peaks ($\omega_\phi = 3715 \text{ cm}^{-1}$) and $\alpha = 0.011$ and $\beta = 1.22$. In the following, we will focus on discussing the IR spectra of $\text{OH}^-(\text{H}_2\text{O})_{n=4-7}$ at two characteristic temperatures (50K and 200K). At 50K, the spectra

are dominated by the most stable isomers shown on the left-hand side in Fig.2. Therefore, the IR spectrum for $\text{OH}^-(\text{H}_2\text{O})_7$ on the left hand side of Fig 3 is the spectrum for the cubic solvated hydroxide.

In Fig. 3, we present the size dependence of the vibrational IR spectra for $\text{OH}^-(\text{H}_2\text{O})_{4-7}$. Compared to the protonated species, there are only limited experimental measurements for the deprotonated $\text{OH}^-(\text{H}_2\text{O})_n$ species. Johnson's group measured IR spectra of $\text{OH}^-(\text{H}_2\text{O})_n$ for $n \leq 5$ ¹⁴ and our simulated spectra of $\text{OH}^-(\text{H}_2\text{O})_5$ at 50K are consistent with their spectra. The most intense peaks in IR spectra are the IHB vibration modes occur below 3250 cm^{-1} . While OH^- in these clusters have all three-coordinated (thus three IHBs), the positions of the IHBs appear to be very sensitive to the hydrogen bond network solvating OH^- . The difference between in the IHBs in $n=4/5$ and $n=6/7$ suggest that the influence is extended to region beyond the first solvation shell. The averaged IR spectra at 200K are shown in Fig. 3(b). At this temperature, we expect co-existence of many structural isomers and the structures of dominating isomers have changed to relatively more open ones. One can find that spectral features of IHB (that is below 3250 cm^{-1}) are substantially broadened due to the co-existence of different structural isomers. Furthermore, the homogenous broadening of these red shifted peaks also contribute to the width in this spectral range. Here it is important to note that the IHB OH stretching modes easily couple with other vibrational modes, such as the OO stretching modes and OH bending modes,^{56,57} therefore one should anticipate that anharmonic coupled vibrational calculations can give a better estimate on the peak positions. However as noted previously, the peaks in the frequency range of $2000\text{-}3200 \text{ cm}^{-1}$ are heavily mixed and one cannot quantify a pure "fundamental" excitation.⁵⁵ On the other hand, all these mixed peaks are borrowing the strong intensity of the IHB stretching mode. Therefore the spectra feature in this region is observed as a broad peak and this contribution is

effectively incorporated using the red shift dependent homogeneous width equation used in the present study. One can clearly notice that in the frequency range of 2300 to 3000 cm^{-1} , as the temperature rises the IR spectra will have a continuum like absorption due to the IHB OH stretching absorption of different isomers.

Next we discuss the 3250 and 3600 cm^{-1} region, which are assigned to the hydrogen bonded O-H stretches in the second/third solvation shell. In the 50 K results for $n=4/5$, peaks are seen at 3500-3600 cm^{-1} , while for $n=6/7$ they are at the 3400-3500 cm^{-1} region. Next, if we compare the IR spectra of the same size at low (50K) and elevated (200K) temperatures, in $\text{OH}^-(\text{H}_2\text{O})_4$, $\text{OH}^-(\text{H}_2\text{O})_5$ and $\text{OH}^-(\text{H}_2\text{O})_6$, we can see new bands appear at around 3250 cm^{-1} . For $\text{OH}^-(\text{H}_2\text{O})_7$, one can clearly find that the averaged oscillator strength in the 3250-3500 cm^{-1} region has red-shifted as temperature increase from 50 to 200K. As mentioned in the section III B, the higher temperature is dominated by isomers which have more open structures (SR and T), where the total number of hydrogen bond has decreased compared to the isomers that dominate at lower temperatures (MR and DR). Since stronger red shifted peaks signify stronger hydrogen bonding, this means that in these open structures the averaged hydrogen bonding strength in the outer solvation shell is stronger than those in more compact structures. This is very counter intuitive since one will imagine that the hydrogen bonding weakens with the increase in temperature. In the present case, the total number of outer solvation shell hydrogen bonding decreases however the hydrogen bonding that are left are stronger. It would be interesting if measurements can be extended both to larger size and to higher temperature to experimentally observe this change in vibrational spectra.

As mentioned above, due to the overwhelming number of 3-coordinated species in the clusters studied in the present study, the spectral features in Fig 3 only contain information on

those species. To obtain understanding in the variation of the first solvation shell, we plot the IR spectra for the 4- and 5- coordinated species in Fig 4. First as seen for $\text{OH}^-(\text{H}_2\text{O})_4$, the IHB peaks for the 4-coordinated isomer shows up at the $3200\text{-}3400\text{ cm}^{-1}$ region. At low temperature, the 3-coordinated $\text{OH}^-(\text{H}_2\text{O})_4$ do not have peaks in that region, therefore the observation of the peaks in that region hint the existence of 4-coordinated $\text{OH}^-(\text{H}_2\text{O})_4$. Next as can be seen from the size dependence in Fig 4(a), the IHB peaks red shift with the increase in number of second solvation shell water. Furthermore, the peaks for the outer shell water show up at the region of $3500\text{-}3600\text{ cm}^{-1}$. For the 5-coordinated species, as seen for $n=6$ and 7, the peaks for the outer water once again show up at 3500 to 3600 cm^{-1} range. Since for the 3-coordinated species the increase in outer shell waters cause peaks to show up in the $3250\text{-}3350\text{ cm}^{-1}$ range, one may experimentally detect the 5 coordinated species by monitoring the high frequency outer shell hydrogen bonded region of $3500\text{-}3600\text{ cm}^{-1}$. We note that since there are only a small number of 4/5 coordinated isomers, the temperature dependence of the 4/5 coordinated species is very small (see supplementary material)

For simple linear molecules it is well known that the selection rule for IR absorption is opposite for Raman scattering. Similarly, for the $\text{OH}^-(\text{H}_2\text{O})_{n=4-7}$ the Raman spectra depicted in Fig.S5 show complementary information to their IR counterparts (shown in Fig.3). The intensity of IHB is significantly suppressed and free OH stretch modes now become intense peaks. This difference in intensity makes it easier to utilize Raman spectra to analyze the spectra features of the free OH as well as the hydroxide stretch. We compile the frequencies and intensities of the free OH stretch of the most stable isomer of $\text{OH}^-(\text{H}_2\text{O})_{n=4-7}$ at 0K in Table I. One can see that the free O-H stretching vibration of hydroxide have relative weaker IR intensity than the free O-H in the solvating waters. However, in Raman scattering, it appears that OH^- has comparable Raman

activity thereby allowing these peaks to be observed. Indeed in aqueous phase, the vibrational spectra of hydroxide stretching vibration only shows up as a hump in IR absorption spectra, but is observed as a strong sharp peak in the Raman scattering spectra.^{8,58}

Concentrating on the peak position of the hydroxide stretching vibration, one can notice that an increase in the number of solvating waters causes a slow but consistent blue shift of the peaks. This is consistent with the studies by Hermansson and coworkers.^{59,60} From the results obtained here, the hydroxide stretching peaks seem to be converging toward a value of 3640 to 3650 cm^{-1} , which is within the range that many aqueous experiments have observed the hydroxide stretching vibration (3610-3640 cm^{-1}). Similar to our previous study²⁹ we notice that the IR absorption intensity for the hydroxide stretching vibration is an order smaller compared to other OH stretching vibrations in the $\text{OH}^-(\text{H}_2\text{O})_{4-7}$ cluster. This was previously shown to be related to the hydration induced stabilization of the excess charge in the hydroxide anion, which is directly related to the vertical detachment energy discussed in the next section.

D. Vertical detachment electronic spectra

In Figure 5, we present the hydration number n dependent VDE spectra for 50 and 200 K calculated using B3LYP and EOM-CCSD IP. One can clearly notice that the general increase of VDE with n can be seen in both methods and the peak positions are within ~ 0.2 eV of each other. This is consistent with the previous studies for smaller size clusters, $n=0-4$, which verified that B3LYP method is able to give 1st VDE energies within 0.1eV of those obtained by higher level CCSD(T) methods when considering clusters which take the tree species.²⁹ Looking at the temperature dependence, at 50 K one can notice that the values seem to saturate at around 6 eV for cluster size larger than 4. On the other hand, at 200K a drastic broadening of

~0.5 eV is seen from the different isomers that coexist for $n > 4$. In Table II, we present the calculated VDE energies for the different topologies for $n = 4-7$. One can clearly notice that the VDE for the more compact (MR and DR) isomers are much smaller than the open (SR and T) species. This general trend is also seen in the 2nd and 3rd VDE presented in Table III. As can be seen from the structures given in Fig 1, many of the open species have the hydrogen bonded OH in the outer solvation shell facing the hydroxide oxygen atom. Thereby this additive contribution from the dipole moments made by the solvating water molecules can stabilize the excess electron around the hydroxide. This notion is consistent with the red shifting seen in the vibrational spectra at higher temperatures. At higher temperatures, the population of the open isomers increase and the outer shell water hydrogen bonding OH stretching peaks show a greater red shift. This is a result of the stronger outer solvation shell interaction caused by facing the negative charge of the hydroxide.

Next in Figure 6 we present the the 2nd and 3rd VDE peaks as well as the 1st one for 50 K and 200 K calculated by the EOM-CCSD IP method using the B3LYP populations. As mentioned in section II C, for the bare OH⁻ the first two excitations are from the degenerate 2p orbitals of the oxygen so are both calculated round 1.8 eV. On the other hand, the 3rd detachment from the Σ orbital is seen much higher at 6 eV. Looking at the 50 K results for the hydrated hydroxide clusters, the energies for the first two detachments split up due to the breaking of the symmetry. However, they are calculated to be within 0.5 eV of each other. The first two peaks increase greatly with n , going from 1.6 eV at $n = 0$ to 6 eV at $n = 5$. On the other hand, the 3rd VDE is already 6 eV at $n = 0$, and stays nearly constant at 7 eV for sizes greater than $n = 3$. In the 200 K results, one can clearly see that the higher energy isomers cause the peaks to broaden. An interesting trend is that the 3rd VDE's not only broadens, but also shows up at much

blue shifted regions, closer to 8 eV for $n=6$ and 7. As mentioned in section III A. the 3-coordinated isomers dominate the present spectra. However previous liquid phase simulation have mentioned the importance of the 4- and 5-coordinated water.^{9,22,59} Therefore similar to the IR spectra (given in Fig 4), we present the VDE spectra for the 4- and 5-coordinated isomers of $\text{OH}^-(\text{H}_2\text{O})_n$ $n = 4-7$ using the population at 200K in Fig 7 (for the result for 50 K see supplementary material). One can clearly notice that the increase in the coordination number of the hydroxide results in a slight blue shifting of the peaks. However, looking at the present results, the VDE of these midsized clusters are much lower than the 9.2 eV observed for the aqueous phase at room temperature.²⁸ On the other hand, as seen in Tables II, the addition of outer solvation water molecules to the 4-coordinated isomer of $\text{OH}^-(\text{H}_2\text{O})_4$ (5.49 eV $n = 4$ T, isomer I) in $\text{OH}^-(\text{H}_2\text{O})_6$ (6.01 eV $n = 6$ T, isomer I) and $\text{OH}^-(\text{H}_2\text{O})_7$ (6.25 eV $n = 7$ T, isomer I) results in a 1.0 eV increase in excitation energy. Since previous studies by Winter et al.²⁸ required a cluster of 20 water molecules to obtain results consistent with bulk results, we are presently pursuing a study on larger cluster system to bridge the gap, and they will be reported in future publications.

CONCLUSIONS

Based on the structures we found using hierarchical search method, we systematically analyzed the structures, relative stability, and thermal dependence of the vibrational and electronic spectra of $\text{OH}^-(\text{H}_2\text{O})_n$ for cluster size $n = 4 - 7$. For $n = 7$, the cubic structure was found to be very stable and it dominates the population for temperature below 200 K. From the results obtained by the harmonic super position approximation, we show that the 3-coordinated species dominate the population. For these 3-coordinated isomers, at low temperatures, compact topologies with

many intermolecular hydrogen bonding in the outer solvation shell dominate the population. However, open topologies with fewer intermolecular hydrogen bonding in outer solvation shell dominate the population at higher temperatures. The interesting point is that while the total number of intermolecular hydrogen bonding decreases for these open isomers, the binding strength of each one hydrogen bond has increased. This can be observed in the increase in the vibrational peaks at the $3200\text{-}3300\text{ cm}^{-1}$ region. Furthermore, in these open species, the outer solvation shell water molecules have hydrogen bonded OH bonds that are facing the negative charged hydroxide. This directional hydrogen bonding causes the binding energy of the excess electron of hydroxide to increase and this can be observed as a blue shifting in the simulated photoelectron spectra calculated from the vertical detachment energy. We hope that these trends in the spectra will be observed experimentally in the future.

Although the present study provides a systematic study on the evolution of vibrational and photoelectron spectra of midsized hydroxide water clusters, the simulated photoelectron spectra were far away from the bulk phase. Further studies on larger clusters should provide more information on the effect of outer solvation shells.



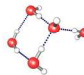
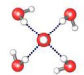
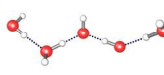
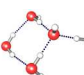
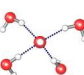
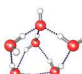
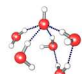
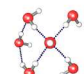

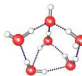
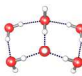
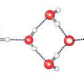

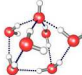
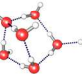
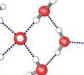
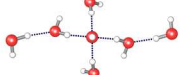
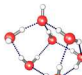
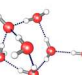
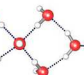
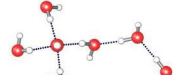
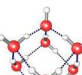
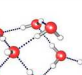
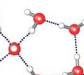
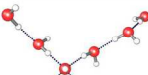
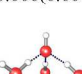
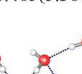
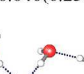
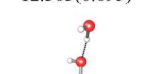
n		MR	DR	SR	TREE	LINEAR
4	I					
			0.000(1.160)	0.003(0.000)	0.536(1.822)	6.159(3.911)
4	II					
				0.009(0.083)	2.196(2.329)	
5	I					
		0.000(0.482)	0.439(1.483)	2.224(2.075)	5.196(2.652)	
5	II					
		0.086(0.532)	0.467(0.000)	2.353(0.799)	5.208(2.209)	
6	I					
		0.000(0.899)	2.825(1.536)	4.234(2.723)	6.799(4.259)	
6	II					
		0.001(0.000)	2.979(1.766)	4.703(2.627)	7.766(5.556)	
7	I					
		0.000(0.000)	6.485(5.380)	8.846(6.237)	12.363(8.895)	
7	II					
		0.594(0.687)	6.823(5.299)	8.899(6.301)	12.866(8.079)	

Figure 1. Low-energy isomers of $\text{OH}^-(\text{H}_2\text{O})_{n=4-7}$, grouped according to their topologies, namely from left to right, MR (multi-ring), DR (double-ring), SR (single-ring), L (linear) and T (tree) and their relative electronic energies (E_0) optimized at B3LYP/6-311+G(d,p). The numbers enclosed in parentheses denote the relative energies with ZPE correction. All values are shown in the unit of kcal/mol.

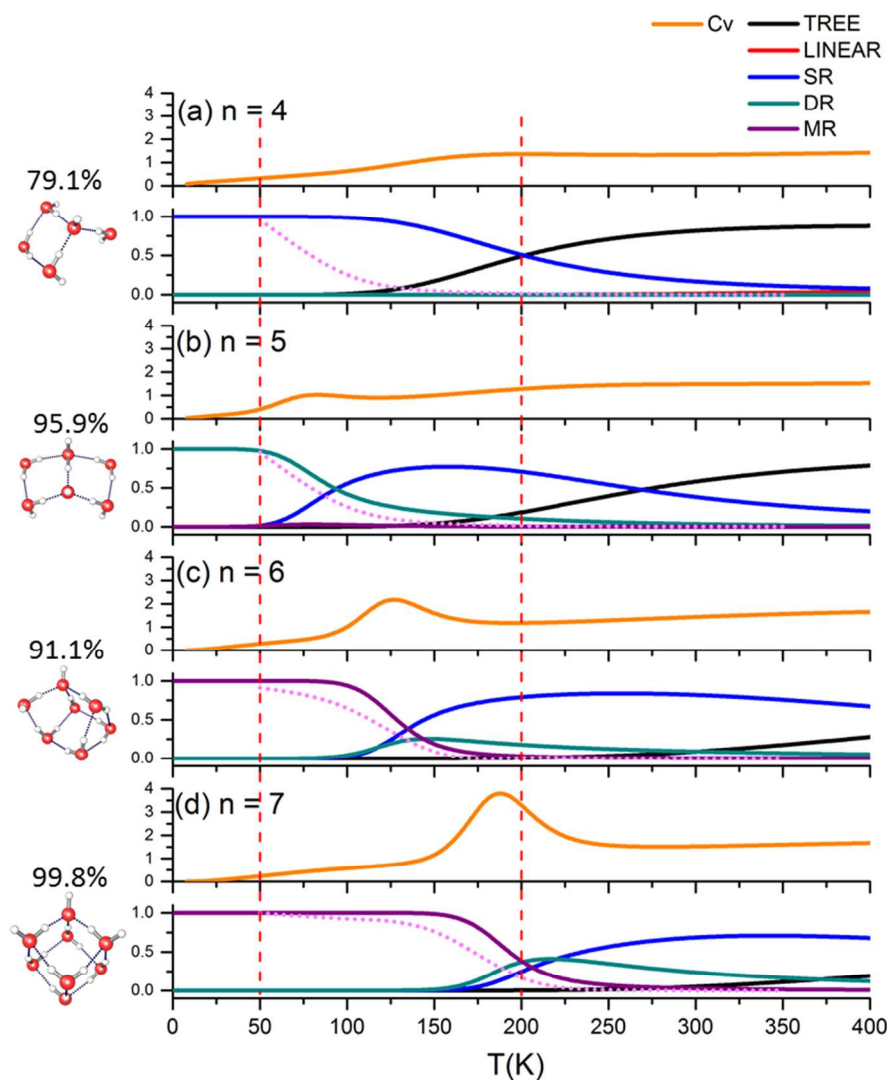


Figure 2. Temperature dependence of heat capacity C_V and population of different topologies for $\text{OH}^-(\text{H}_2\text{O})_{4-7}$. The hump in $C_V(T)$, shown as orange lines in upper panels, is associated with structural change. Populations of five topological groups (shown in lower panels) are calculated using HSA based on energetics and vibrational frequencies with B3LYP/6-311+G(d,p). Tree, Linear, Single Ring, Double Ring, and Multi Ring are given by black, red, blue, green and violet lines. At 0K, there is only one isomer which is given schematically on the left hand for each $\text{OH}^-(\text{H}_2\text{O})_{4-7}$. We present the population of this isomer with dotted pink lines. The red lines drawn at 50 K and 200 K are for guiding the eyes.

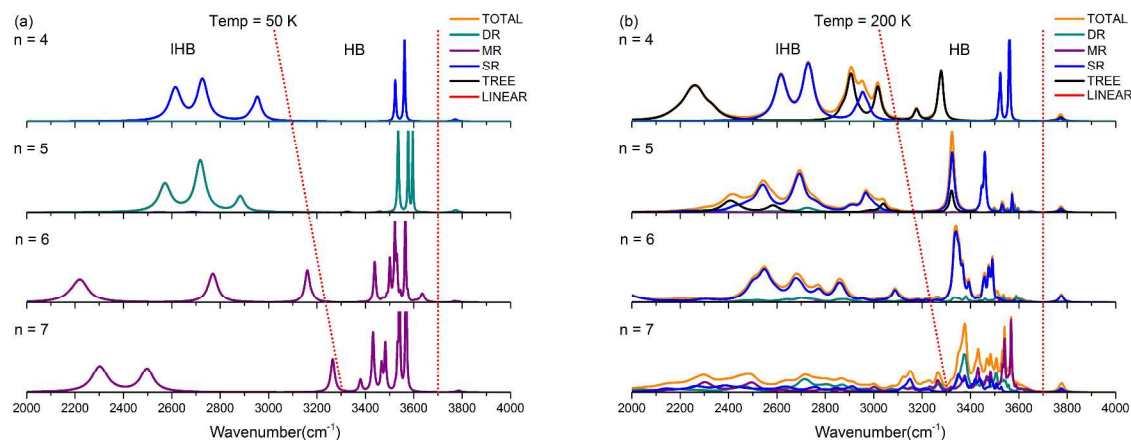


Figure 3. IR spectra of $\text{OH}^-(\text{H}_2\text{O})_{n=4-7}$ at two characteristic temperatures (50K and 200K). At 50K, the spectra are dominated by the most stable isomers shown in Fig.2. The IHBs peaks appear below 3250 cm^{-1} and are very sensitive to the local geometry of the water molecules in the first solvation shell. In between 3250 to 3600 cm^{-1} are the hydrogen bonded O-H stretching of waters in the outer solvation shell. Contributions from Tree, Linear, Single Ring, Double Ring, and Multi Ring isomers are given by black, red, blue, green and violet lines.

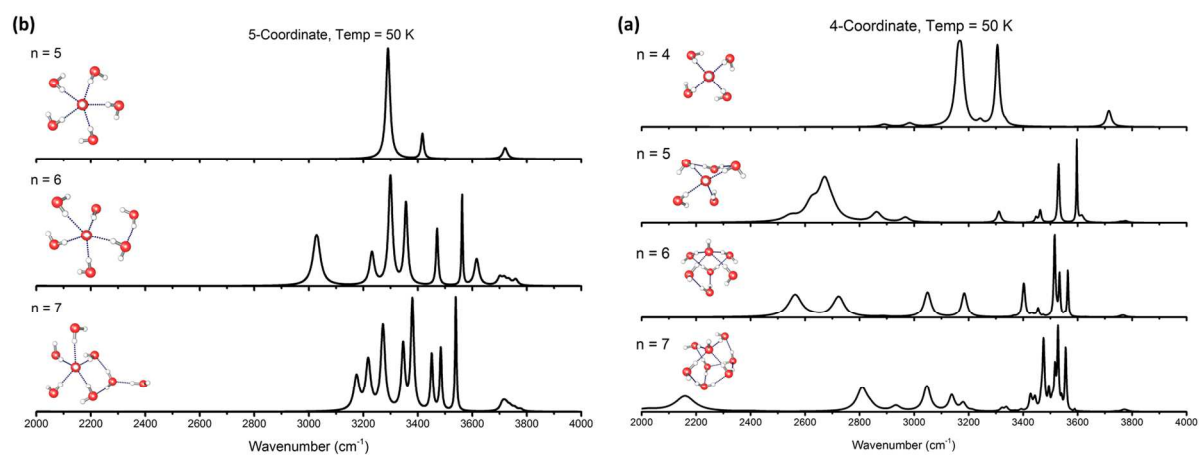


Figure 4. IR spectra of $\text{OH}^-(\text{H}_2\text{O})_{n=4-7}$ for the (a) 4- and (b) 5-coordinated isomers calculated using the population at 50 K. Representative structures for the isomers are depicted in the figures.

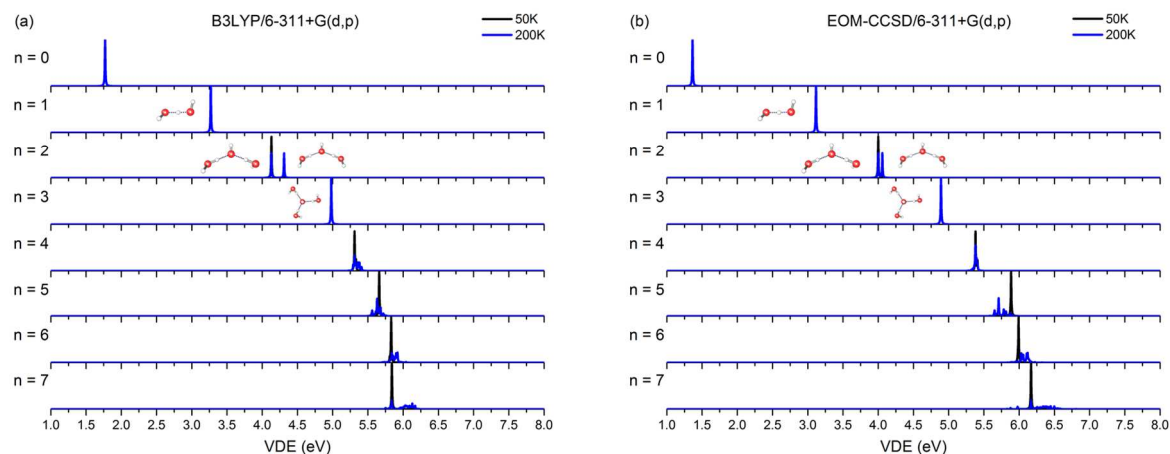


Figure 5. Vertical electron detachment spectra of $\text{OH}^-(\text{H}_2\text{O})_{n=4-7}$ at two characteristic temperatures calculated using B3LYP and EOM-CCSD methods. The results for 50K and 200K are given in black and blue, respectively. For smaller species, $n < 4$, we present the isomers responsible for the observed transitions. For $n > 4$ see Fig. 2 for the dominant isomers.

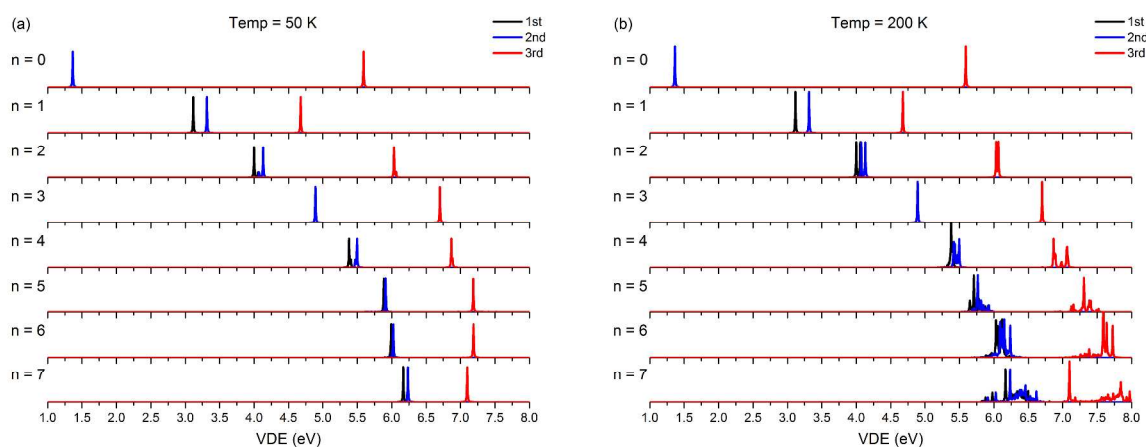


Figure 6. The 1st, 2nd, and 3rd vertical electron detachment spectra of $\text{OH}^-(\text{H}_2\text{O})_{n=4-7}$ at two characteristic temperatures (50K and 200K) calculated using EOM-CCSD methods. The results for 1st, 2nd, and 3rd are given in black, blue, and red, respectively.

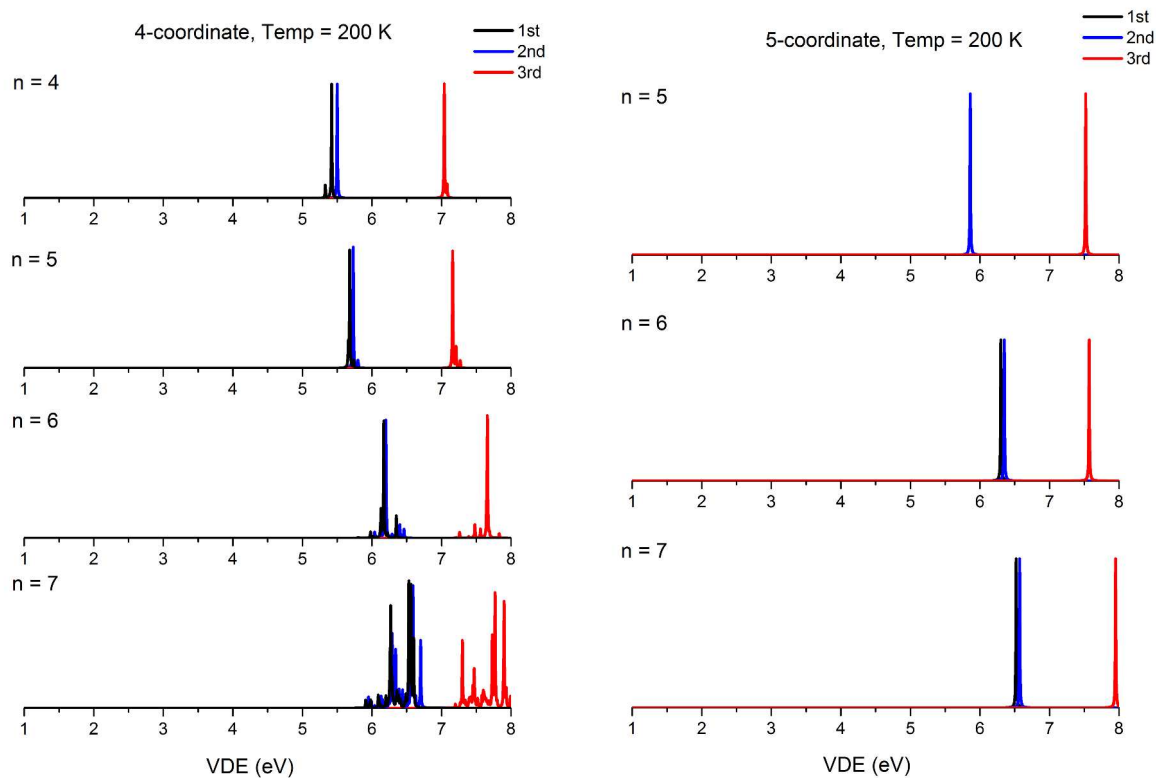


Figure 7. The 1st, 2nd, and 3rd vertical electron detachment spectra of $\text{OH}^-(\text{H}_2\text{O})_{n=4-7}$ at 200 K calculated using EOM-CCSD methods for the 4 and 5-coordinated species. See Figure 4 for schematic structures.

Table I. Peak position, in cm^{-1} , IR intensity, in km mol^{-1} , and Raman activity, in $\text{\AA}^4 \text{amu}^{-1}$, of the free OH stretch of the most stable isomers of $\text{OH}^-(\text{H}_2\text{O})_{n=4-7}$. The structures of these isomers are depicted in Figure 2.

	n = 4			n = 5			n = 6			n = 7		
	Peak Pos.	IR Int.	Raman Activ.	Peak Pos.	IR Int.	Raman Activ.	Peak Pos.	IR Int.	Raman Activ.	Peak Pos.	IR Int.	Raman Activ.
OH^-	3620.3	0.2	91.3	3623.8	1.7	86.4	3639.5	1.2	107.6	3643.1	1.7	116.7
Free OH	3640.8	1.7	37.6	3641.1	22.5	57.2	3509.9	199.8	47.9	3655.0	28.2	65.3
	3641.8	2.6	30.6	3643.8	2.3	0.2	3637.8	20.6	50.4	3655.5	9.6	155.5
	3642.2	4.3	75.0	3644.4	30.8	125.7	3653.3	15.1	97.8			

Units: Frequency (cm^{-1}), IR intensity (KM/mole), and Raman activity ($\text{\AA}^4/\text{amu}$)

Table II. 1st VDE, in eV, calculated using the B3LYP and EOM-CCSD IP for the two most stable isomers for different topologies. The structures of these isomers are depicted in Figure 1.

		VDE			
		n = 4	n = 5	n = 6	n = 7
		B3LYP (EOM-CCSD)			
MR	I	-	5.60 (5.64)	5.88 (5.98)	5.84 (6.17)
	II	-	5.56 (5.61)	5.83 (5.99)	5.75 (5.88)
DR	I	5.26 (5.22)	5.72 (5.66)	5.81 (5.95)	6.14 (6.30)
	II	-	5.66 (5.89)	5.83 (5.99)	6.10 (6.38)
SR	I	5.31 (5.38)	5.74 (5.68)	6.00 (6.13)	6.08 (6.27)
	II	5.33 (5.41)	5.63 (5.71)	6.04 (6.17)	6.09 (6.29)
TREE	I	5.49 (5.33)	5.66 (5.69)	6.01 (6.12)	6.25 (6.40)
	II	5.46 (5.42)	5.68 (5.78)	5.97 (5.98)	6.26 (6.55)
LINEAR	I	5.17 (5.19)	-	-	-

II - - - -

Table III. 2nd and 3rd VDE, in eV, calculated using the EOM-CCSD IP for the two most stable isomers for different topologies. The structures of these isomers are depicted in Figure 1.

		VDE			
		n = 4	n = 5	n = 6	n = 7
		2 nd VDE / 3 rd VDE			
MR	I	-	5.66 / 6.97	6.04 / 7.26	6.24 / 7.10
	II	-	5.68 / 6.98	6.02 / 7.19	5.91 / 7.18
DR	I	5.33 / 6.82	5.72 / 7.21	6.02 / 7.32	6.33 / 7.65
	II	-	5.91 / 7.19	6.01 / 7.44	6.44 / 7.64
SR	I	5.50 / 6.87	5.73 / 7.16	6.17 / 7.65	6.36 / 7.89
	II	5.47 / 6.88	5.77 / 7.31	6.20 / 7.66	6.38 / 7.89
TREE	I	5.33 / 7.08	5.77 / 7.44	6.18 / 7.83	6.41 / 7.93
	II	5.50 / 7.04	5.81 / 7.39	6.01 / 7.58	6.59 / 8.13
LINEAR	I	5.36 / 6.92	-	-	-
	II	-	-	-	-

AUTHOR INFORMATION

Corresponding Author

‡ Ren-Jie Lin and Quoc Chinh Nguyen contributed equally to this study.

*Email: kt@gate.sinica.edu.tw and jlkuo@pub.iam.s.sinica.edu.tw

ACKNOWLEDGMENT

This research is financially supported by Academia Sinica, Nanyang Technological University and the Ministry of Science and Technology of Taiwan (Grant: MOST102-2113-M-001-012-MY3 and MOST101-2113-M-001-023-MY3). RJL would like to thank Mr. Ying-Cheng Li and Mr. En-Ping Lu for their technical assistance. We would like to thank the generous allocation of computational resources provided by National Center for High-performance Computing and Academia Sinica Computing Center.

REFERENCES

- 1 J. D. Bernal and R. H. Fowler, *J. Chem. Phys.*, 1933, **1**, 515.
- 2 T. Megyes, S. Bálint, T. Grósz, T. Radnai, I. Bakó and P. Sipos, *J. Chem. Phys.*, 2008, **128**, 044501.
- 3 S. Imberti, A. Botti, F. Bruni, G. Cappa, M. A. Ricci and A. K. Soper, *J. Chem. Phys.*, 2005, **122**, 194509.
- 4 C. D. Cappa, J. D. Smith, B. M. Messer, R. C. Cohen and R. J. Saykally, *J. Phys. Chem. A*, 2007, **111**, 4776–85.
- 5 E. F. Aziz, N. Ottosson, M. Faubel, I. V Hertel and B. Winter, *Nature*, 2008, **455**, 89–91.
- 6 T. Corridoni, A. Sodo, F. Bruni, M. A. Ricci and M. Nardone, *Chem. Phys.*, 2007, **336**, 183–187.
- 7 M. Śmiechowski and J. Stangret, *J. Mol. Struct.*, 2007, **834-836**, 239–248.
- 8 S. T. Roberts, P. B. Petersen, K. Ramasesha, A. Tokmakoff, I. S. Ufimtsev and T. J. Martinez, *Proc. Natl. Acad. Sci. U. S. A.*, 2009, **106**, 15154–9.
- 9 M. E. Tuckerman, *Science (80-.)*, 1997, **275**, 817–820.
- 10 L. I. Yeh, M. Okumura, J. D. Myers, J. M. Price and Y. T. Lee, *J. Chem. Phys.*, 1989, **91**, 7319.
- 11 M. Okumura, L. I. Yeh, J. D. Myers and Y. T. Lee, *J. Phys. Chem.*, 1990, **94**, 3416–3427.
- 12 M. Miyazaki, A. Fujii, T. Ebata and N. Mikami, *Science*, 2004, **304**, 1134–7.

- 13 J.-W. Shin, N. I. Hammer, E. G. Diken, M. A. Johnson, R. S. Walters, T. D. Jaeger, M. A. Duncan, R. A. Christie and K. D. Jordan, *Science*, 2004, **304**, 1137–40.
- 14 W. H. Robertson, E. G. Diken, E. A. Price, J.-W. Shin and M. A. Johnson, *Science*, 2003, **299**, 1367–72.
- 15 J. A. Fournier, C. J. Johnson, C. T. Wolke, G. H. Weddle, A. B. Wolk and M. A. Johnson, *Science*, 2014, **344**, 1009–12.
- 16 X. Yang and A. W. Castleman, *J. Phys. Chem.*, 1990, **94**, 8500–8502.
- 17 A. Vegiri and S. V. Shevkunov, *J. Chem. Phys.*, 2000, **113**, 8521.
- 18 S. S. Xantheas, *J. Am. Chem. Soc.*, 1995, **117**, 10373–10380.
- 19 H. M. Lee, P. Tarkeshwar and K. S. Kim, *J. Chem. Phys.*, 2004, **121**, 4657–64.
- 20 A. B. McCoy, X. Huang, S. Carter and J. M. Bowman, *J. Chem. Phys.*, 2005, **123**, 64317.
- 21 X. Li, V. E. Teige and S. S. Iyengar, *J. Phys. Chem. A*, 2007, **111**, 4815–20.
- 22 X. Sun, S. Yoo, S. S. Xantheas and L. X. Dang, *Chem. Phys. Lett.*, 2009, **481**, 9–16.
- 23 A. Bankura and A. Chandra, *Chem. Phys.*, 2012, **400**, 154–164.
- 24 E. A. Price, W. H. Robertson, E. G. Diken, G. H. Weddle and M. A. Johnson, *Chem. Phys. Lett.*, 2002, **366**, 412–416.
- 25 G. C. C. Y. S. W. J. C. J. Y. T. L. H. C. Chang, *Mol. Phys.*, 2001, **99**, 1161–1173.
- 26 M. Morita and K. Takahashi, *Phys. Chem. Chem. Phys.*, 2013, **15**, 114–24.
- 27 P. J. Linstrom and W. G. Mallard, *J. Chem. Eng. Data*, 2001, **46**, 1059–1063.
- 28 B. Winter, M. Faubel, I. V Hertel, C. Pettenkofer, S. E. Bradforth, B. Jagoda-Cwiklik, L. Cwiklik and P. Jungwirth, *J. Am. Chem. Soc.*, 2006, **128**, 3864–5.
- 29 M. Morita, H. Takahashi, S. Yabushita and K. Takahashi, *Phys. Chem. Chem. Phys.*, 2014, **16**, 23143–9.
- 30 Q. C. Nguyen, Y. S. Ong, H. Soh and J.-L. Kuo, *J. Phys. Chem. A*, 2008, **112**, 6257–61.
- 31 Q. C. Nguyen, Y.-S. Ong and J.-L. Kuo, *J. Chem. Theory Comput.*, 2009, **5**, 2629–2639.
- 32 L. Ojamäe, I. Shavitt and S. J. Singer, *J. Chem. Phys.*, 1998, **109**, 5547.

- 33 B. Bandow and B. Hartke, *J. Phys. Chem. A*, 2006, **110**, 5809–22.
- 34 Y. S. Ong and A. J. Keane, *IEEE Trans. Evol. Comput.*, 2004, **8**, 99–110.
- 35 A. D. Becke, *J. Chem. Phys.*, 1993, **98**, 5648.
- 36 C. Lee, W. Yang and R. G. Parr, *Phys. Rev. B*, 1988, **37**, 785–789.
- 37 A. D. McLean and G. S. Chandler, *J. Chem. Phys.*, 1980, **72**, 5639.
- 38 R. Krishnan, J. S. Binkley, R. Seeger and J. A. Pople, *J. Chem. Phys.*, 1980, **72**, 650.
- 39 T. Clark, J. Chandrasekhar, G. W. Spitznagel and P. V. R. Schleyer, *J. Comput. Chem.*, 1983, **4**, 294–301.
- 40 M. J. Frisch, J. A. Pople and J. S. Binkley, *J. Chem. Phys.*, 1984, **80**, 3265.
- 41 P. J. Ballester and W. G. Richards, *Proc. R. Soc. A Math. Phys. Eng. Sci.*, 2007, **463**, 1307–1321.
- 42 M. J. Frisch, G. W. Trucks, H. B. Schlegel, G. E. Scuseria, M. A. Robb, J. R. Cheeseman, G. Scalmani, V. Barone, B. Mennucci, G. A. Petersson, H. Nakatsuji, M. Caricato, X. Li, H. P. Hratchian, A. F. Izmaylov, J. Bloino, G. Zheng, J. L. Sonnenberg, M. Hada, M. Ehara, K. Toyota, R. Fukuda, J. Hasegawa, M. Ishida, T. Nakajima, Y. Honda, O. Kitao, H. Nakai, T. Vreven, J. A. Montgomery Jr., J. E. Peralta, F. Ogliaro, M. Bearpark, J. J. Heyd, E. Brothers, K. N. Kudin, V. N. Staroverov, R. Kobayashi, J. Normand, K. Raghavachari, A. Rendell, J. C. Burant, S. S. Iyengar, J. Tomasi, M. Cossi, N. Rega, J. M. Millam, M. Klene, J. E. Knox, J. B. Cross, V. Bakken, C. Adamo, J. Jaramillo, R. Gomperts, R. E. Stratmann, O. Yazyev, A. J. Austin, R. Cammi, C. Pomelli, J. W. Ochterski, R. L. Martin, K. Morokuma, V. G. Zakrzewski, G. A. Voth, P. Salvador, J. J. Dannenberg, S. Dapprich, A. D. Daniels, O. Farkas, J. B. Foresman, J. V Ortiz, J. Cioslowski and D. J. Fox, .
- 43 Y.-S. Wang, H.-C. Chang, J.-C. Jiang, S. H. Lin, Y. T. Lee and H.-C. Chang, *J. Am. Chem. Soc.*, 1998, **120**, 8777–8788.
- 44 P. L. Polavarapu, *J. Phys. Chem.*, 1990, **94**, 8106–8112.
- 45 F. Calvo, J. P. . Doye and D. . Wales, *Chem. Phys. Lett.*, 2002, **366**, 176–183.
- 46 T. V Bogdan, D. J. Wales and F. Calvo, *J. Chem. Phys.*, 2006, **124**, 044102.
- 47 J. Douady, F. Calvo and F. Spiegelman, *J. Chem. Phys.*, 2008, **129**, 154305.
- 48 F. H. Stillinger and T. A. Weber, *Phys. Rev. A*, 1982, **25**, 978–989.

- 49 F. H. Stillinger and T. A. Weber, *Science*, 1984, **225**, 983–9.
- 50 D. J. Wales, *Mol. Phys.*, 2006, **78**, 151–171.
- 51 D. Wales, *Energy Landscapes: Applications to Clusters, Biomolecules and Glasses*, Cambridge University Press, 2003.
- 52 D. Sinha, S. K. Mukhopadhyay, R. Chaudhuri and D. Mukherjee, *Chem. Phys. Lett.*, 1989, **154**, 544–549.
- 53 M. Nooijen and R. J. Bartlett, *J. Chem. Phys.*, 1995, **102**, 3629.
- 54 Y. Shao, L. F. Molnar, Y. Jung, J. Kussmann, C. Ochsenfeld, S. T. Brown, A. T. B. Gilbert, L. V Slipchenko, S. V Levchenko, D. P. O'Neill, R. A. DiStasio, R. C. Lochan, T. Wang, G. J. O. Beran, N. A. Besley, J. M. Herbert, C. Y. Lin, T. Van Voorhis, S. H. Chien, A. Sodt, R. P. Steele, V. A. Rassolov, P. E. Maslen, P. P. Korambath, R. D. Adamson, B. Austin, J. Baker, E. F. C. Byrd, H. Dachsel, R. J. Doerksen, A. Dreuw, B. D. Dunietz, A. Dutoi, T. R. Furlani, S. R. Gwaltney, A. Heyden, S. Hirata, C.-P. Hsu, G. Kedziora, R. Z. Khallulin, P. Klunzinger, A. M. Lee, M. S. Lee, W. Liang, I. Lotan, N. Nair, B. Peters, E. I. Proynov, P. A. Pieniazek, Y. M. Rhee, J. Ritchie, E. Rosta, C. D. Sherrill, A. C. Simmonett, J. E. Subotnik, H. L. Woodcock, W. Zhang, A. T. Bell, A. K. Chakraborty, D. M. Chipman, F. J. Keil, A. Warshel, W. J. Hehre, H. F. Schaefer, J. Kong, A. I. Krylov, P. M. W. Gill and M. Head-Gordon, *Phys. Chem. Chem. Phys.*, 2006, **8**, 3172–91.
- 55 M. Morita and K. Takahashi, *Phys. Chem. Chem. Phys.*, 2012, **14**, 2797–808.
- 56 J. S. Mancini and J. M. Bowman, *Phys. Chem. Chem. Phys.*, 2015, **17**, 6222–6.
- 57 K. Mackeprang, V. Hänninen, L. Halonen and H. G. Kjaergaard, *J. Chem. Phys.*, 2015, **142**, 094304.
- 58 N. B. Librovich, V. P. Sakun and N. D. Sokolov, *Chem. Phys.*, 1979, **39**, 351–366.
- 59 K. Hermansson, P. A. Bopp, D. Spångberg, L. Pejov, I. Bakó and P. D. Mitev, *Chem. Phys. Lett.*, 2011, **514**, 1–15.
- 60 P. D. Mitev, P. A. Bopp, J. Petreska, K. Coutinho, H. Ågren, L. Pejov and K. Hermansson, *J. Chem. Phys.*, 2013, **138**, 064503.